TELLES TRANSFORMATION APPLIED TO THE EVALUATION OF 3D ANISOTROPIC FUNDAMENTAL SOLUTION

Anderson Gabriel Santiago, gsantiago@fem.unicamp.br
Paulo Sollero, sollero@fem.unicamp.br
Eder Lima de Albuquerque, ederlima@fem.unicamp.br
University of Campinas, UNICAMP - R. Mendeleiev, 200 CEP 13083-870

Abstract. This paper presents an application of the Telles Transformation for the evaluation of the three dimensional elastostatics anisotropic fundamental solution. This solution is obtained by numerical integration using gaussian quadrature. For high levels of anisotropy, the numerical integration is quite expensive, since a very large number of integration points is needed. The Telles transformation is applied in order to decrease the Gauss-Legendre sample points and keep a good accuracy.

Keywords: Telles transformation; Anysotropic elastostatics; Numerical integration; Boundary element method

1. INTRODUCTION

The fundamental solution for 3D anisotropic elastostatics has only integral terms and it is difficult to find a closed form. The use of complex variables was first proposed by Cruse and Sweldlow (1971) for 2D problems, and since then, it has been extensively used for this kind of analysis (Deb and Banerjee, 1990; Deb, 1996). Vogel and Rizzo (1973) also presents a solution for 3D problems and Schclar (1994) also presents a study using the Fourier transform for 3D problems. This formulation implies a huge computational effort, which is undesirable since the calculation of the matrices $[H]$ and $[G]$ takes most part of the time of the analysis. Phan et al. (2005) presents a formulation using a residue approach for the calculus of this fundamental solution and Benedetti et al. (2008) make use of an Adaptative Cross Aproximation (ACA) to speed up the calculations of the influence matrices for a 3D isotropic case.

This paper presents a study and a first effort to decrease the time of calculating the fundamental solution by applying the Telles transform and by doing so, decrease the number of sample points used to integrate the functions of the tensors u_{ij}^* and t_{ij}^*. It shows that, depending on the material properties, the application of the Telles transform leads to a very accurate result with fewer sample points than those used in an ordinary integration using Gauss-Legendre quadrature.

2. THE 3D ANISOTROPIC FUNDAMENTAL SOLUTION

The fundamental solution is needed in order to evaluate the Eq. (1) only over the boundary of the problem, Γ. For isotropic elasticity, such functions can be found for example, in Aliabadi (2002); Banerjee (1994); Beer (2001); Kane (1994), which are closed form functions. For transversely isotropic media, the fundamental solution was first developed by Pan and Chou (1976), then Loloi (2000) treated the singularities and proposed a new form of evaluating these functions by rearranging each one according to the direction of the applied load. For anisotropic elastostatics, Wilson and Cruse (1978) developed a numerical fundamental solution applying the Fourier transform to the equilibrium equation written as a function of the displacements, as can be seen in Eq. (2). Then, the inverse transform is obtained only by numerical integration.

$$\int_\Gamma u_{ij}^* t_j d\Gamma = \int_\Gamma t_{ij}^* u_j d\Gamma + u_j(\xi) \tag{1}$$

$$C_{ijkl} \frac{\partial^2 u_{mk}^*}{\partial x_l \partial x_j} = -\delta_{im}\delta(\boldsymbol{r}) \tag{2}$$

where C_{ijkl} is the compliance tensor, t_j and u_j are the nodal surafce forces and displacements, δ_{ij} is the Kronecker delta, $\boldsymbol{r}$ is the distance vector between the source point and the field point and ξ is the source point.

An easier approach is found in Gaul et al. (2003), where the authors apply the Radon transform to Eq. (2) and the fundamental solution for displacements is obtained by the inverse transform. Equation (3) shows the u_{mk}^*, obtained by applying the inverse Radon transform. This equation is a two dimensional integration, performed over the surface of a unit sphere (Fig. 2). It must be noticed that the integrand of Eq. (3) has a Dirac's Delta representation, and thus, it can be rewritten as a one dimensional integration over a unit circle shown in Fig. 2. leading to Eq. (4). In Eq. (5) the vector z_i is given by Eq. (6) where vector α is orthogonal to β, and both are orthogonal to r^0, which is the normalized distance vector.

$$u_{mk}^* = \frac{1}{8\pi^2 r} \int_{z_i z_i = 1} \left[M_{jm}^{zz}(z_i) \right]^{-1} \delta(z_i r_i^0) \, d\Gamma(z_i) \tag{3}$$

$$= \frac{1}{8\pi^2 r} \oint_0^{2\pi} \left[M_{jm}^{zz} \left(z_i \right) \right]^{-1} d\phi \tag{4}$$

$$M_{jm}^{zz} \left(z_i \right) = C_{ijkl} z_j z_l \tag{5}$$

$$z_i = \alpha_i cos \left(\phi \right) + \beta_i sin \left(\phi \right) \tag{6}$$
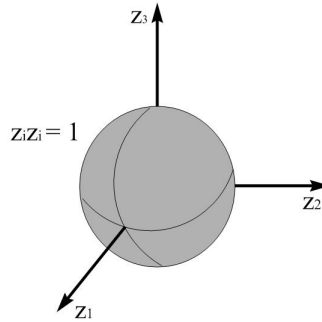
Figure 1. Unit sphere for the inverse Radon transform.
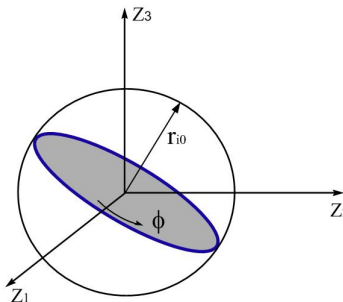
Figure 2. Unit circle for the integration of the fundamental solution.

In order to evaluate Eq. (4), the Gauss-Legendre quadrature is used. For an isotropic material, few sample points are needed to lead to a good accuracy. But for transversely isotropic and anisotropic materials, several points are needed.

Studies made in the GMCMCb (Computational Modelling of Composite and Biomaterials Group) (Santiago, 2008) at UNICAMP, shows that in some cases, 80 sample points are necessary for good results (errors of order 10^{-12}). Therefore, in order to decrease the number of sample points, the authors applied the Telles transformation, aiming to concentrate the integration points around a critical point and increase the speed of the calculations.

3. THE TELLES TRANSFORMATION

The Telles transformation (Telles, 1987) is a polynomial based transformation which intends to concentrate the points of integration around a critical point, where the function tends to high values.

It is applied to the normalized domain, Eq. (7).:

$$I = \int_{-1}^{1} f \left(\xi \right) d\xi \tag{7}$$

where in Eq. (8), $J \left(\xi \right)$ is the jacobian of the transformation between the real domain to the normalized domain.:

$$f \left(\xi \right) = g \left(x \left(\xi \right) \right) J \left(\xi \right) \tag{8}$$

$$-1 \leq \xi \leq 1$$

Considering a second degree polynomial in Eq. (9):

$$\xi \left(\gamma \right) = a\gamma^2 + b\gamma + c \tag{9}$$

Its coefficients are determined by imposing the restrictions given by Eq. (10) to Eq. (12):

$$\xi\left(1\right) \quad = \quad 1 \tag{10}$$

$$\xi\left(-1\right) \quad = \quad -1 \tag{11}$$

$$\left.\frac{d\xi}{d\gamma}\right|_{\bar\xi} \quad = \quad 0 \tag{12}$$

where $\bar\xi$ is the singular point of $f\left(\xi\right)$. The coefficients are given by Eq. (13) to Eq. (15):

$$a \quad = \quad -c \tag{13}$$

$$b \quad = \quad 1 \tag{14}$$

$$c \quad = \quad \frac{\bar\xi \pm \sqrt{\bar\xi^2 - 1}}{2} \tag{15}$$

It must be noticed that $||\bar\xi|| \leq 1$ in order to avoid complex roots. A third degree polynomial can be used, and doing so, the transformation becomes general, independently of the value of $\bar\xi$. In this case, another condition given by Eq. (16) must be satisfied.

$$\left.\frac{d^2\xi}{d\gamma^2}\right|_{\bar\xi} = 0 \tag{16}$$

This condition implies that polynomial $\xi\left(\gamma\right)$ has its maximum (or minimum) at $\bar\xi$.

For this new function, Eq. (17) is a third order polynomial and its coefficientes given by Eq.(18) to Eq. (23):

$$\xi\left(\gamma\right) = a\gamma^3 + b\gamma^2 + c\gamma + d \tag{17}$$

$$a \quad = \quad \frac{1}{Q} \tag{18}$$

$$b \quad = \quad -\frac{3\bar\gamma}{Q} \tag{19}$$

$$c \quad = \quad \frac{3\bar\gamma^2}{Q} \tag{20}$$

$$d \quad = \quad -b \tag{21}$$

$$Q \quad = \quad 1 + 3\bar\gamma^2 \tag{22}$$

$$\bar\gamma \quad = \quad \sqrt[3]{\bar\eta\eta^* + |\eta^*|} + \sqrt[3]{\bar\eta\eta^* - |\eta^*|} + \bar\eta \tag{23}$$

The integral defined by Eq. (7) is rewritten as follows in Eq. (24) and the new jacobian in Eq. (25):

$$I \quad = \quad \int_{-1}^{1} f\left[\xi\left(\gamma\right)\right] J^*\left(\gamma\right)\, d\gamma \tag{24}$$

$$J^*\left(\gamma\right) \quad = \quad \frac{d\xi}{d\gamma} \tag{25}$$

The sample points for Gauss-Legendre integration are redistributed around $\bar\gamma$.

For example, considering function $f\left(\xi\right) = -log\left(|\xi - \frac{2}{3}|\right)$, Fig. 3 shows the distribution of the integration points with and without the Telles transformation using the third degree polynomial.
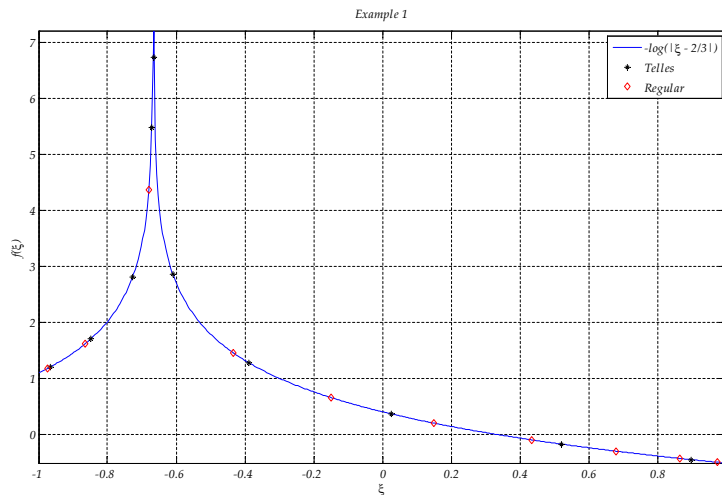
Figure 3. Distribution of the sample points around a critical point.

4. INTEGRATION OF THE 3D ANISOTROPIC FUNDAMENTAL SOLUTION USING THE TELLES TRANS-FORMATION

The Telles transformation was applied in three cases, considering the level of anisotropy of the material.

At this point it is interesting to study how the transformation can be used to integrate periodical functions, since as shown in Eq. (6), the fundamental solution for 3D anisotropic elastostatics is a periodical function, depending on $sin\phi$ and $cos\phi$.

To illustrate the use of the transform, let's consider two different cases:

1. $I_1 = \int_0^\pi \left[sin\left(x\right) + cos\left(x\right) \right] \, dx$;

2. $I_2 = \int_0^{0.49\pi} tan\left(x\right) \, dx$;

Considering the first example, Fig. 4 shows the integrand of I_1. The points of integration are concentrated at the maximum of the curve, i. e., at $x = \frac{\pi}{4}$.
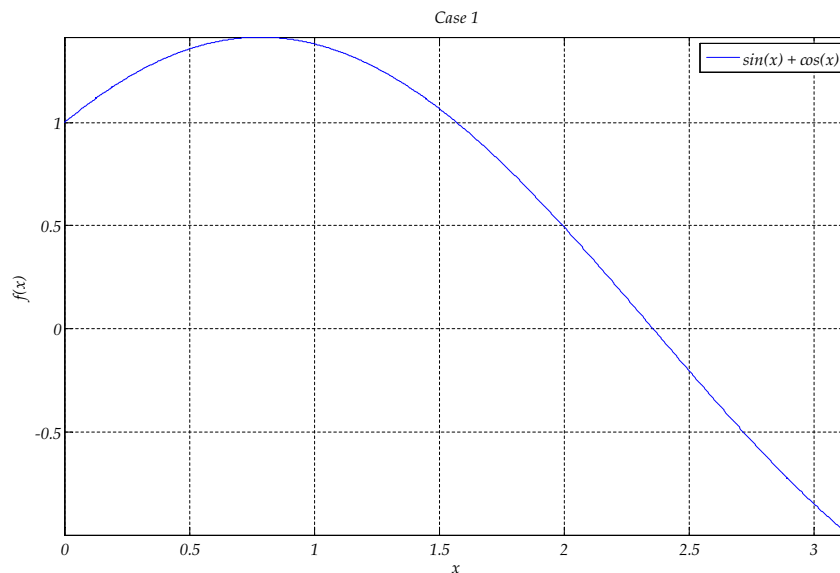
Figure 4. First example: $g\left(x\right) = sin\left(x\right) + cos\left(x\right)$

For the above case, the integration was performed using 10 and 30 sample points. The results, considering a maximum error of 10^{-14}, are shown in Tab. 1.

Table 1. Comparison between the use of the Telles transformation and regular integration. Case 1.

	10 sample points	30 sample points
$Error_{reg}$	2.775557×10^{-13}	3.330669×10^{-14}
$Error_{Telles}$	5.799473×10^{-5}	6.328271×10^{-13}

For the second case, the integrand is shown in Fig. 5, and the integration points are concentrated at $x = 0.49\pi$:
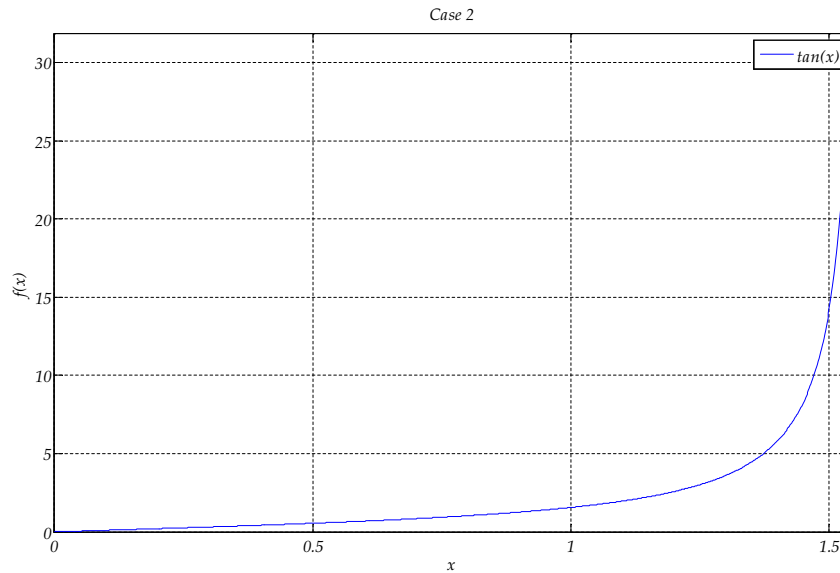
Figure 5. Second example: $g(x) = tan(x)$

The results for 10 and 30 sample points are :

Table 2. Comparison between the use of the Telles transformation and regular integration: Case 2

	10 sample points	30 sample points
$Error_{reg}$	4.186832×10^{-1}	2.137277×10^{-6}
$Error_{Telles}$	2.137277×10^{-3}	7.526381×10^{-11}

For the first case, where the first derivative does not undergo abrupt changes, the regular integration procedure works better than the one with the use of the Telles transformation. On the other hand, the second case, where several variations of the function occur, the transfomation induces a high efficient integration process.

Bearing such results in mind, the results of the integration of the 3D fundamental solution can be more easily understood.

In order to find the critical point, i. e., the coordinate where the sample points should be concentrated, an optimization process was used: the Golden section search, which does not use derivatives. This method was chosen over gradient-based methods like Newton-Raphson, because the second derivative of the tensor components according to ϕ undergoes high values, greater than the values obtained from the first derivative. So, the step of each iteration towards the optimum point is very small, leading to a divergent result or taking too many iterations to achieve the optimum point.

Considering element G_{31}^u, the distance vector $\mathbf{d} = (1, 1, 5)$, the curves of the component according to the variable of integration ϕ and the distribution of the sample points with and without the application of Telles transformation, along the comparison of the numerical results follows :

4.1 Graphite-epoxy (monoclinic)

For the first case, considering a monoclinic graphite-epoxi, the compliance tensor is:

$$[C] = \begin{bmatrix} 95.50 & 28.90 & 4.03 & 0.00 & 0.00 & 44.70 \\ 28.90 & 25.90 & 4.65 & 0.00 & 0.00 & 15.60 \\ 4.03 & 4.65 & 16.30 & 0.00 & 0.00 & 0.54 \\ 0.00 & 0.00 & 0.00 & 4.40 & -1.78 & 0.00 \\ 0.00 & 0.00 & 0.00 & -1.78 & 6.45 & 0.00 \\ 44.70 & 15.60 & 0.54 & 0.00 & 0.00 & 32.70 \end{bmatrix} GPa \tag{26}$$

The distribution of the sample points with and without the transformation can be seen in Fig. 6.
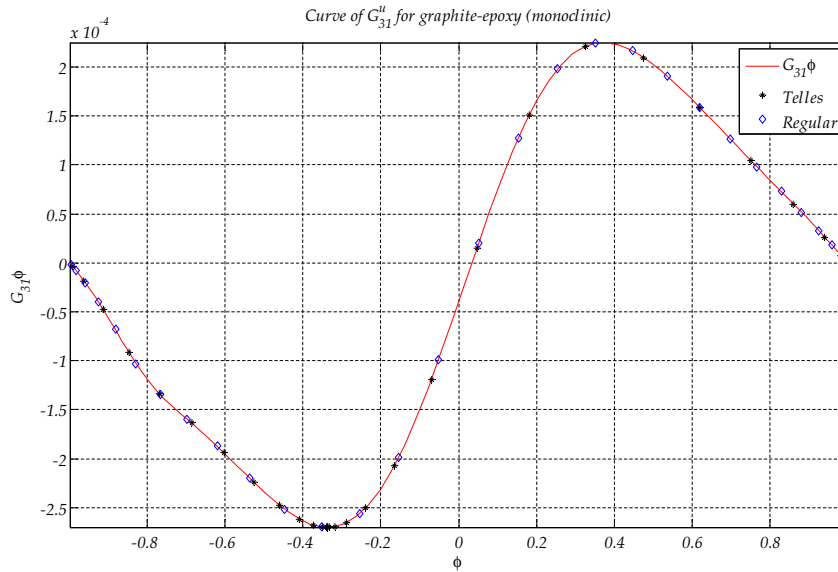
Figure 6. Curve $G_{31}^u (\phi)$ for graphite-epoxy.

In this case, the contribution of the use of the transformation leads to a very poor integration, making the use of the regular procedure more effective. Table 3 shows the numerical results for this example, taking as a reference value the integration using 100 sample points on the regular integration.:

Table 3. Numerical results for graphite-epoxy.

	Regular integration	Telles
Error (40 sample points)	1.325998×10^{-7}	2.041891×10^{-5}
Error (50 sample points)	6.846356×10^{-10}	2.576511×10^{-7}

4.2 PZT (transversely isotropic)

The second case presents a study of PZT (piezoelectric material). The compliance tensor is given by Eq. (27) and the curve for $G_{31}^u (\phi)$ along with the distribution of the sample points in Fig. 7:

$$[C] = \begin{bmatrix} 107.60 & 63.10 & 63.90 & 0.00 & 0.00 & 0.00 \\ 63.10 & 107.60 & 63.90 & 0.00 & 0.00 & 0.00 \\ 63.90 & 63.90 & 100.40 & 0.00 & 0.00 & 0.00 \\ 0.00 & 0.00 & 0.00 & 19.60 & 0.00 & 0.00 \\ 0.00 & 0.00 & 0.00 & 0.00 & 19.60 & 0.00 \\ 0.00 & 0.00 & 0.00 & 0.00 & 0.00 & 22.20 \end{bmatrix} GPa \tag{27}$$
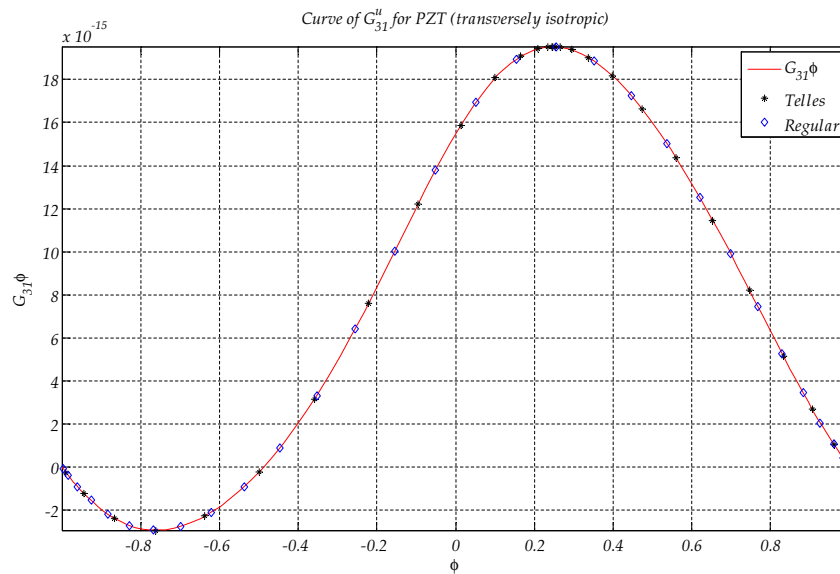
Figure 7. Curve $G_{31}^u (\phi)$ for PZT.

Table 4. Numerical results for PZT.

	Regular Integration	Telles
Error (40 sample points)	6.060665×10^{-14}	4.040443×10^{-13}
Error (50 sample points)	4.040443×10^{-14}	3.636399×10^{-13}

As was observed in the previous case, the transformation does not improve the accuracy of the results, leading to a poorer integration than the regular one.

4.3 Spruce (orthotropic)

Finally, the third case presents the study of an orthotropic material (spruce). The compliance tensor and the distribution of the sample points are given below:

$$[C] = \begin{bmatrix} 0.44 & 0.32 & 0.19 & 0.00 & 0.00 & 0.00 \\ 0.32 & 16.27 & 0.45 & 0.00 & 0.00 & 0.00 \\ 0.19 & 0.45 & 0.78 & 0.00 & 0.00 & 0.00 \\ 0.00 & 0.00 & 0.00 & 0.61 & 0.00 & 0.00 \\ 0.00 & 0.00 & 0.00 & 0.00 & 0.039 & 0.00 \\ 0.00 & 0.00 & 0.00 & 0.00 & 0.00 & 0.76 \end{bmatrix} GPa \quad (28)$$
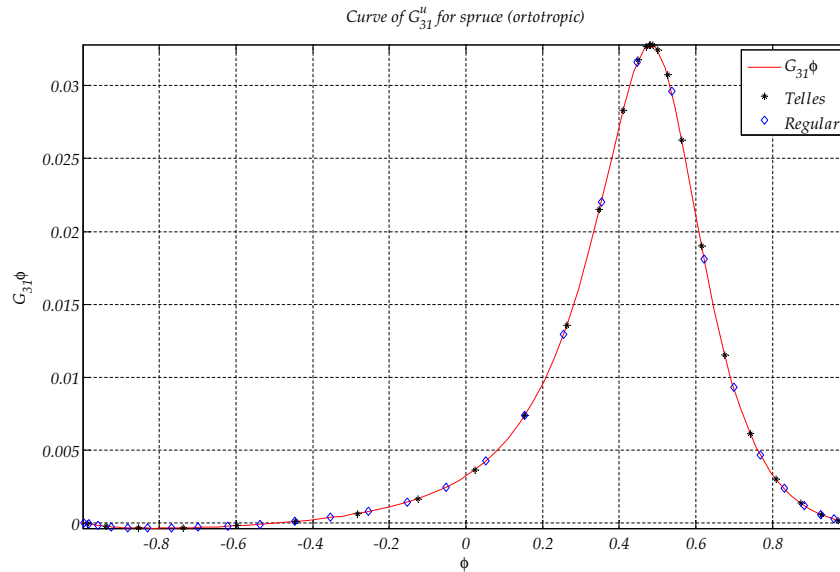
Figure 8. Curve $G_{31}^{u}(\phi)$ for spruce.

As discussed earlier in this section, the behavior of the curve of this material can be compared to the second example $(g(x) = tan(x))$. This curve has high values for the first order derivatives. Thus, Telles transformation works better when compared to the previous cases. Table 5 shows the improvement obtained by using the transformation.

Table 5. Numerical results for spruce.

	Regular integration	Telles
Error (40 sample points)	4.097811×10^{-5}	1.421271×10^{-9}
Error (50 sample points)	9.823273×10^{-7}	3.956622×10^{-13}

Some interesting points can be noticed here:

1. The use of the transformation greatly improves the accuracy of the integration;

2. About the material properties, some elements of the compliance tensor are greater than others ($C_{22}/C_{33} = 20.858974$; $C_{22}/C_{55} = 4.171794 \times 10^2$);

3. The improvement caused by the transformation tends to a limit value, as can be seen in Fig. 4.3
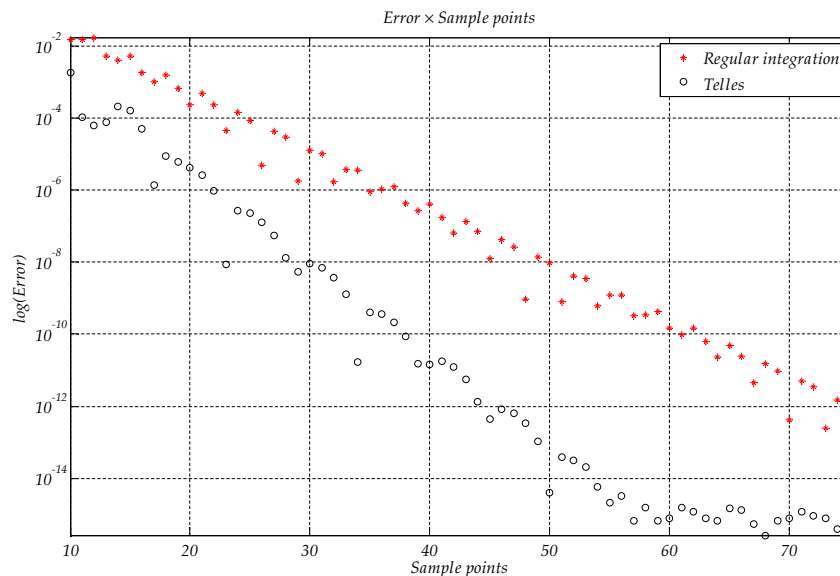
Figure 9. Error with and without the Telles transformation.

5. CONCLUSIONS

By means of the study made in this article, Telles transformation does not apply in all cases for integration of the 3D anisotropic fundamental solution, but the cases in which it can be applied, it highly improves the integration process, leading to errors of order 10^{-8} with fewer sample points than those which would take a regular integration.

Now efforts have been made to develop a rule to determine in which cases the transformation can be applied without being necessary to analyse the curves of the fundamental solution tensor, for example, analysing the frequency response of the material.

6. ACKNOWLEDGEMENTS

The authors would like to thank CNPq (*National Council of Scientific and Technological Development*, Brazil) for the financial support.

References

Aliabadi, M. H. (2002). *The Boundary Element Method - Vol. 2*. John Wiley & Sons.

Banerjee, P. K. (1994). *The Boundary Element Methods in Engeneering*. McGraw Hill Book Company.

Beer, G. (2001). *Programing the Boundary Element Method - An Introduction to Engineers*. John Wiley & Sons.

Benedetti, I., Aliabadi, M. H., and Davì, G. (2008). A fast 3d dual boundary element method based on hierarchical matrices. *International Journal of Solids and Structures*, 45:2355 – 2376.

Cruse, T. A. and Sweldlow, J. L. (1971). Interactive program for analysis and design problems in advanced composites. Technical report, Carnegie-Mellon University.

Deb, A. (1996). Boundary elements analysis of anisotropic bodies under thermo mechanical body force loadings. *Computers and Structures*, 58:715 – 726.

Deb, A. and Banerjee, P. K. (1990). Bem for general anisotropic 2d elasticity using particular integrals. *Communications in Applied Numerical Methods*, 6:111 – 119.

Gaul, L., Kögl, M., and Wagner, M. (2003). *Boundary Element Methods for Engineers and Scientists: An Introductory Course with Advanced Topics*. Springer.

Kane, J. H. (1994). *Boundary Element Analysis in Engineering Continuum Mechanics*. Prentice-Hall, Inc.

Loloi, M. (2000). Boundary integral equation solution of three-dimensional elastostatic problems in transversely isotropic solids using closed-form displacement fundamental solutions. *Int. J. Numer. Meth. Engng, John Wiley & Sons, Ltd.*, 48:823 – 842.

Pan, Y. C. and Chou, T. W. (1976). Point force solution for an infinite transversely isotropic solid. *Journal of Applied Mechanics, Transactions of the ASME*, 43:608–612.

Phan, A. V., Gray, L. G., and Kaplan, T. (2005). Residue approach for evaluating the 3d anisotropic elastic green's function: multiple roots. *Engineering Analysis With Boundary Elements*, 29:570 – 576.

Santiago, A. G. (2008). Análise de problemas de anisotropia 3d com sub-regiões utilizando o método dos elementos de contorno. Master's thesis, University of Campinas.

Schclar, N. A. (1994). *Anisotropic Analysis Using Boundary Elements*. Computational Mechanics Publications.

Telles, J. C. F. (1987). A self-adaptative co-ordinate transformation for efficient numerical evaluation of general boundary element integrals. *International Journal for Numerical Methods in Engineering*, 24:959 – 973.

Vogel, S. M. and Rizzo, F. J. (1973). An integral equation formulation of three dimensional anisotropic elastostatic boundary value problems. *J. of Elasticity*, 3:203 – 216.

Wilson, R. B. and Cruse, T. A. (1978). Efficient implentation of anisotropic three dimensional boundary integral equation stress analysis. *Int. J. Numer. Meth. Engn*, 12:1383 – 1397.

7. Responsibility notice

The authors are the only responsible for the printed material included in this paper.